Keratin–polyethylene oxide bio-nanocomposites reinforced with ultrasonically functionalized graphene†

M. Grkovic,[a] D. B. Stojanovic,*[b] A. Kojovic,[b] S. Strnad,[c] T. Kreze,[c] R. Aleksic[b] and P. S. Uskokovic[b]

Polyethylene oxide (PEO) functionalized graphene (f-G) was prepared by ultrasonication of pristine graphene in PEO aqueous solution. The feasible sonication protocol of PEO degradation and graphene functionalization enabled fabrication of solvent cast nanocomposites. Additionally, the steps to form new bio-nanocomposite films have been described. Taking the advantage of the combination of graphene, PEO and keratin fibers from poultry feather waste, the aforementioned bio-nanocomposite films were designed with extraordinary properties allowing the films to have promising applications as eventual packaging materials and enabling bio-waste keratin to be converted into value-added materials. Compared to neat PEO, addition of only 0.3 wt% f-G provided an increase of 92% to the storage modulus. These findings are similar to the nanoindentation results, which yielded increases in the reduced modulus of the same composition by about 92%. Nanoindentation testing shows that the incorporation of 0.3 wt% f-G increased the reduced modulus and hardness of the keratin–PEO blend by about 155 and 99%, respectively.

1. Introduction

Green chemistry has become a new perspective for the prevention of pollution in an economically feasible way through the use of chemicals and processes that are environmentally friendly. Chicken feathers from poultry production are natural renewable sources of the fibrous protein, keratin.[1] In green chemistry, keratin has found uses in films, packaging, building materials and bioplastics.[2–4] Keratin has also found applications in membrane devices for separation and adsorption[5,6] and has biomedical applications[7–9] in different forms, such as films, hydrogels, sponges, fibers and scaffolds.[10] Functional groups within the keratin structure enable strong intermolecular interactions, therefore the poor mechanical properties, especially the fragile nature of pure keratin and the low solubility in most used solvents, could be overcome by functionalization[11,12] and mixing keratin with other polymers, natural or synthetic, like chitosan, cellulose, gelatin, fibroin, nylon, PEO, PLLA and similar.[7,13–19] A new approach is to graft carbon nanotubes and graphene structures with keratin, or generally speaking, to modify carbon structures with natural polymers,[20–22] which provides a possibility of producing bio-nanocomposites.

Polyethylene oxide is a low cost, commercially available biodegradable material, with favorable mechanical features and processability. Due to its high polarity, this material is compatible with a large number of chemical substances, solvents and polar nanofillers with applications in biomedicine[23,24] and in electrolytes within lithium batteries and solar cells.[25–27] Changing the structure of PEO with irradiation, which produces macromolecules with radical end groups and stimulates recombination with cleaved polymer chains, provides a new perspective for the application of this polymer.[28–30]

Due to their outstanding thermal, electrical and mechanical properties, graphene sheets are used in a wide range of applications such as in electrical devices, solar cells and, as in our study, as reinforcements in composite films.[31–36] A new application of the graphene structure could be incorporation in polymer blend systems.[37] The advantages and benefits of graphene's application are provided when graphene is in very low content.[38–40] The use of organic polymers with both low and high molecular weight, mixed with graphene, provide manufacturing materials with superior characteristics.[41–43] Most researchers based their work on the transformation of the inert graphene surface, improving it with various chemical, radical or oxidation reactions. These methods usually involve multi-phase

[a]*Innovation Centre, University of Belgrade, Faculty of Technology and Metallurgy, Belgrade, Serbia. E-mail: duca@tmf.bg.ac.rs; Fax: +381 11 3370387; Tel: +381 11 3303754*

[b]*University of Belgrade, Faculty of Technology and Metallurgy, Belgrade, Serbia*

[c]*University of Maribor, Faculty of Mechanical Engineering, Slovenia*

organic synthesis, which is often very time consuming and sometimes economically inefficient. The use of ultrasound for graphene was limited to mechanical and physical effects, but recently, high intensity ultrasound through the possibility of chemical treatment has provided activation of the inert graphene surface in a feasible manner.[44-48] Incorporation of graphene structures in multicomponent systems has not been sufficiently investigated, and as such opens many possibilities for the production of composite films, especially if one of the components represents a renewable resource. Currently, to the best of our knowledge, there have been no reports on graphene functionalization with PEO using ultrasonic irradiation and no reports on the incorporation of functionalized graphene (f-G) within PEO. Furthermore, in this research the application of feather keratin as an additional linking polymer in the keratin–PEO nanocomposite was thoroughly investigated. Keratin is a naturally derived polymer and due to its biocompatibility and biodegradability it allows biomedical applications of composites with the keratin phase. Due to the similarity with the host tissue, the amino acid sequences of keratin interact and support cellular attachment and proliferation.[1,49] This promotes such composites to be good candidates for wound dressings, scaffolds, drug delivery or water filtration. This would contribute to increasing the need for renewable waste materials and production of biodegradable composites, which could be used as good substitutes for traditional nanocomposites.

In this study, we report the ultrasound functionalization of graphene with a polymer with a high molecular weight and degree of disintegration (PEO), which resulted in a shorter period of ultrasonic treatment. The functionalization with PEO was shown to be an effective method for grafting onto graphene surfaces. The f-G was successfully incorporated in PEO and the keratin–PEO blend, yielding composites with an exceptionally high increase in mechanical properties.

2. Experimental

2.1. Materials

In the experiment, polyethylene oxide (PEO), molecular weight $M_w = 600\,000$ g mol^{-1} (ACROS Organics), and graphene nano platelets (Cheap Tubes, plazma-argon, 1–2 μm diameter, >99 wt% of purity) were used as purchased. Deionized water (DI) (resistance of 18 MΩ cm) was used for the preparation of solutions. Keratin obtained from chicken feathers (waste from a poultry plant – Perutnina Ptuj, Slovenia), in an aqueous solution of 23.15 g L^{-1}, was used for the preparation of composite films.

2.2. Extraction of keratin from chicken feathers

Keratin was obtained from chicken feathers through the process of extraction. Waste feathers were subjected to pretreatment, which involved washing, drying and fine milling to a size of 0.5 mm. For removal of fatty acids, feathers were soaked in a Soxhlet extractor in petrol ether for 12 h at 40–60 °C. To complete the evaporation of petrol ether, feathers were dried in a vacuum oven for 24 h. Then the obtained feathers were

treated with an aqueous solution of urea, mercaptoethanol and sodium dodecyl sulfate (SDS). The derived extract was filtered and dialyzed with cellulose membranes (MWCO 6000–8000 Da) for 72 h, yielding the aqueous solution of keratin. The keratin concentration of the dialysate was determined using a protein assay kit, based on the Hartree–Lowry assay.[50] The keratin solution was stored at 5 °C until application.

2.3. Grafting graphene using ultrasound

0.5 g of polymer (PEO) was dissolved in 100 mL of deionized water (DI) for 2 h until the polymer was completely dissolved, and then the solution was treated with ultrasound (Sonics Vibra Cell VCX 750 W, 19 mm Ti horn) at 22 kHz and 300 W for 2 h while maintaining the temperature at 30 °C.[44] At specified time intervals, a part of the solution was taken to monitor the degree of degradation through changes of the viscosity. Within the process of polymer degradation, the optimal condition of irradiation treatment was determined. Considering the optimal conditions, 0.5 g of PEO was dissolved in DI water. After 2 h, the solution, with an addition of 50 mg pristine graphene (p-G), was vigorously stirred for 40 min and then ultrasonically treated at 22 kHz and 300 W for 70 min with a constant temperature of 30 °C. The resulting mixture was centrifuged at 2000 rpm for 20 min, decanted and centrifuged again at 2000 rpm for 30 min, in order to remove p-G in the form of black sediment. The obtained black solution with dissolved f-G was filtered (200 nm) under vacuum, and washed 3 times with DI water to remove ungrafted PEO. Fig. 1 presents a schematic illustration of the functionalization.

2.4. Preparation of nanocomposite films

Nanocomposite films were obtained using a simple solution casting method on a glass surface. Firstly, neat PEO (0.5 g) was dissolved in DI water for at least 2 h on a magnetic stirrer at 40 °C. When the solution became transparent, pristine graphene (p-G) was added until the graphene content reached 0.3 wt%. The mixture was stirred for 12 h before solvent casting. The composite films with f-G were prepared in the same manner as p-G. The keratin–PEO blend was obtained by dissolving PEO for 2 h, followed by mixing with a keratin solution to a content ratio of 90/10 (keratin–PEO) for 6–12 h at 40 °C. Other content ratios of keratin–PEO are also prepared (95/5, 40/60, 60/40, 5/95; see ESI†) as confirmation of the benefits proposed by the 90/10 ratio blend (in further text marked as keratin–PEO). The bio-nanocomposite keratin–PEO/f-G film was prepared firstly by forming the polymer blend and then subsequently adding 0.3 wt% of f-G into the polymer blend. The mixture was stirred for 12 h before solvent casting. The formed blends were poured in Petri dishes and dried in an oven at 40 °C for 48 h, and then in a vacuum oven at 50 °C for another 12 h.

3. Characterization

Elemental analyses were performed using a VARIO EL III Elemental analyzer.
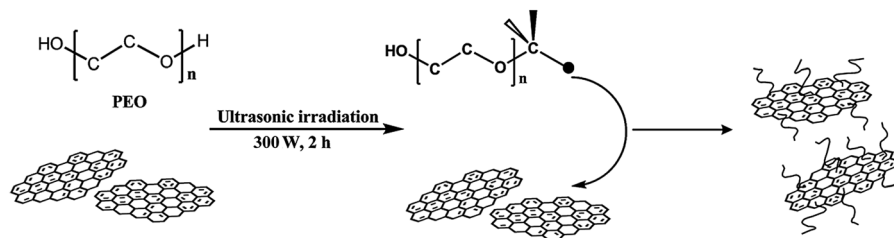
Fig. 1 Schematic illustration of the functionalization of graphene.

Fourier transform infrared (FTIR) spectra were recorded in the 4000–400 cm^{-1} range on a BOMEM spectrophotometer (Hartmann & Braun, MB-series), using the KBr wafer technique. Structural changes of the polymer with ultrasonic treatment and the structure of composites were identified with optical microscopy (Olympus CX41).

Thermal properties of PEO films were examined in a nitrogen atmosphere from room temperature to 80 °C at a heating rate of 10 °C min^{-1} using a differential scanning calorimeter (DSC, Q10 TA Instruments, USA). To determine the melting temperature (T_m), melting enthalpy (ΔH_m) and the degree of crystallinity (χ_m) samples were heated to 80 °C and kept for 10 min. Then they were reheated at a heating rate of 10 °C min^{-1}. Melting temperatures (T_m) were measured from the second cycle as the temperature at the top of the endothermic peak, $T_{m(max)}$. The area under the endothermic peak determined the melting enthalpy, ΔH_m. The degree of crystallinity of films (χ_m) was determined from DSC analysis based on eqn (1):

$$\chi_{m,PEO} = \frac{\Delta H_{m,PEO}}{\Delta H^{\circ}_{m,PEO}\omega} \qquad (1)$$

where $\Delta H_{m,PEO}$ is the melting enthalpy of PEO, $\Delta H^{\circ}_{m,PEO}$ is the melting enthalpy of 100% crystalline PEO (213.7 J g^{-1}) for the PEO molecular weight of 600 000 g mol^{-1},[30] and ω is the mass fraction of PEO.

Thermogravimetric analysis (TGA) was performed using a SDT Q600 simultaneous DSC-TGA instrument (TA Instruments). Samples were heated from room temperature to 600 °C at a heating rate of 10 °C min^{-1} under a nitrogen atmosphere.

The morphology of the fracture surface of composite films obtained with liquid nitrogen was observed by a field emission scanning electron microscope (FESEM), (JSM 5800, Tescan Mira 3), operated at 2 kV.

The nanoindentation experiments on neat polymer and composite films were performed using a Triboscope T950 Nanomechanical Testing System (Hysitron, Minneapolis, MN) equipped with a Berkovich indenter type with an *in situ* imaging mode. A peak load of 2 mN was applied for all samples with a load–hold–unload of 10–20–10 s for each segment. Nine indentation measurements were performed for each sample and the average values and standard deviations are reported.

Dynamic mechanical analysis (DMA, Q800 TA Instruments, USA) was performed successively through two different procedures, both in the film tension clamp mode. The first procedure was performed in the multi frequency mode, with the frequency range from 0.1–10 Hz, in an isothermal condition of 30 °C and with an initial amplitude of 1 μm, in order to determine frequency effects on the storage modulus. After the first procedure, the second procedure was consequently performed so the storage modulus from the end of procedure one was the initial storage modulus of the second procedure, and then another sample was measured. The second procedure was performed in order to determine temperature effects on the storage modulus and tan δ. The temperature ranged from 30 °C to 120 °C with a heating rate of 3 °C min^{-1}, with a constant frequency of 1 Hz and amplitude of 15 μm. The sample size was approximately 40 mm × 5 mm × 0.2 mm.

4. Results and discussion

4.1. Elemental analysis of keratin

Elemental analysis of neat keratin determined a content of 12.78% of N and 3.72% of S. This confirmed a "hard keratin" content of sulfur, which is >3% according to Tonin *et al.*[51] Keratin is known to have an amphoteric character owing to the presence of amino and carboxylic functional groups in the molecular structure. The point of zero charge of feather keratin determined by the titration method was pH 5. The pH value of the keratin solution and blend solutions prepared with it was ≈8, because at this pH most functional groups were deprotonated, which enabled favorable linking with other components in the blends.

4.2. Structural and thermal analysis of grafted graphene

FTIR spectroscopy was used to reveal interactions in f-G between graphene and PEO attached to the graphene surface
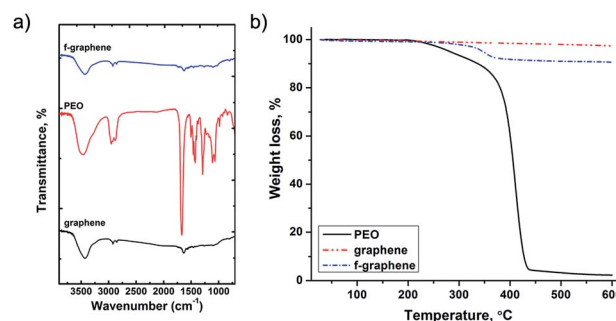

Fig. 2 (a) FTIR spectra and (b) TGA analysis of pristine graphene, neat PEO and functionalized graphene.

(Fig. 2a). FTIR analysis of p-G showed stretching at 2921 and 2815 cm^{-1} due to a C–H methylene group and the peak at $\approx$ 3426 cm^{-1} is due to a hydroxyl group. The peak at 1634 cm^{-1} is also due to the vibration of the deformation of a hydroxyl group, which matches the skeletal vibration of stretching C=C bonds within the graphene structure. Due to terminal hydrogen groups, the FTIR spectrum of neat PEO showed stretching at 3429 cm^{-1}. Spectra also revealed symmetric and asymmetric stretching vibrations from a methylene group. The strong peak at 1670 cm^{-1} belongs to the deformation of the terminal hydrogen group of the PEO macromolecule. Peaks at 1460, 1143, 984 and 840 cm^{-1} are from the CH$_2$ group (scissoring) and its deformation (twisting and wagging). Asymmetric and symmetric stretching of the –C–O–C– ether chain appears at 1389 and 1111 cm^{-1}. The FTIR spectrum of f-G displayed weak interactions between PEO and graphene, but the electrostatic and hydrogen bonding indicated that changes had occurred without destroying the shape or characteristics of the composed materials. Changes at 1630 cm^{-1} refer to the stretching interaction between the aromatic C=C graphene skeleton and aliphatic PEO structure.

In Fig. 2b the weight loss of p-G is about 3%, due to the adsorbed moisture on the graphene surface. The comparative TGA analysis of p-G, PEO and f-G determined that the content of PEO decorating the graphene surface within f-G is about 7.7%.

DSC analysis of the degree of crystallinity indicated that 60 minutes of ultrasonic irradiation was needed for functionalization. With a further increase of the ultrasonic time the DSC parameter values decreased (see Fig. 3a and Table 1, ESI†) due to the cleavage of C–C bonds under polymer chains, which

Table 1 DSC and TGA analyses of composite films

Sample	ΔH_m (J g^{-1})	T_m (°C)	χ_m	Residual mass at 600 °C (%)
PEO	149.0	64.44	0.70	2.28
PEO/p-G	117.3	64.83	0.55	1.11
PEO/f-G	114.8	66.75	0.53	3.07
Keratin–PEO/f-G	—	—	—	18.5

suggests partial or complete polymer degradation. This observation of the crystallinity increase was followed by optical microscopy (Fig. 3b–f), which revealed growth of spherulites with the increase of the ultrasound treatment period. Therefore, the use of ultrasonic irradiation provides PEO chain radicals, through polymer degradation, and produces reactive places on the graphene surface, induced by ultrasonic cavitation. Also, high intensity ultrasound by shear forces enables exfoliation of graphene into single- or few-layer sheets.[44–47] So, this one step functionalization by ultrasonic irradiation provides soluble f-G compared to insoluble p-G in water, suggesting covalent grafting of PEO chains onto the graphene surface, rather than plain physisorption. Also, Fig. S1 (see Fig. S1 ESI†) reveals a favorable dispersion of f-G, without agglomerates associated with the addition of p-G into PEO. Shen and coworkers in their study used a polymer with a low molecular weight and degree of disintegration for functionalization of graphene. Within our research we demonstrated the possibility of using a polymer with a higher molecular weight and degree of disintegration, which resulted in a shorter time of ultrasonic irradiation than the one found in the literature.[44] This functionalization proved to be effective, because it is easy to process, less time consuming and resulted in a good dispersion of f-G in polar solvents.

4.3. Structural and morphological analysis of composite films

Fig. 4 shows FTIR spectra of composite films of: neat PEO, PEO with functionalized graphene, keratin and the keratin–PEO/f-G hybrid (FTIR spectra of all composite films of neat PEO, PEO/p-G, PEO/f-G, keratin, keratin–PEO and keratin–PEO/f-G are given in Fig. S2 in ESI†).

Addition of f-G in the keratin–PEO blend system revealed some changes and new signals between 1400 and 800 cm^{-1} wavenumbers. The appearance of signals at 1400, 1346 and 847 cm^{-1}, detected in the PEO/f-G composite, and new signals at 990 and 920 cm^{-1} suggested asymmetric and symmetric vibrations of ether C–O–C bonds and CH$_2$ group deformation (twisting and wagging) of the polymer towards amide III and carbonyl groups on the protein. These signals confirmed bonding within constituents, beside the enhanced intermolecular hydrogen bonding between the nanofiller (f-G) and polymer blend.

Comparative analysis of SEM and optical microscopy of the composite films (Fig. 5 and S3 ESI†) revealed the influence of the crystallinity on composite films, which resulted in an improvement of mechanical features. Optical images of composite films with both pristine graphene and f-G show
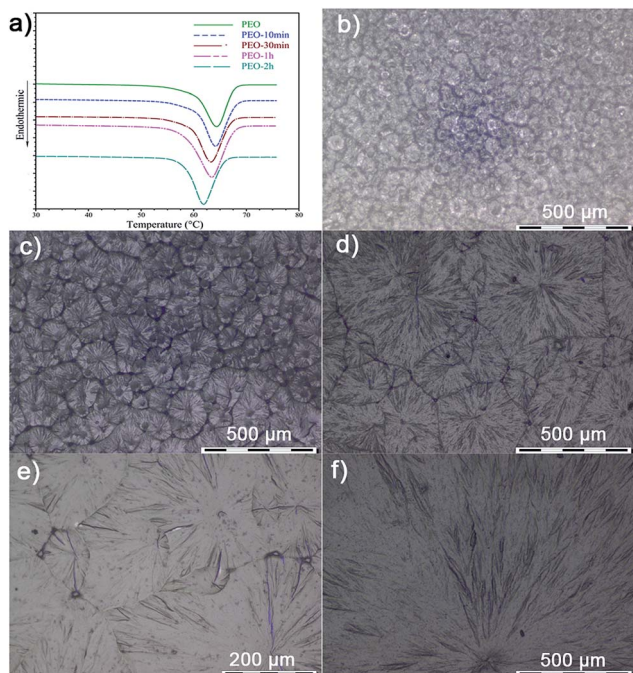

Fig. 3 (a) DSC analysis and (b–f) optical microscopy images of crystalline changes of PEO after 0, 10, 30, 60 and 120 min of ultrasound treatment.
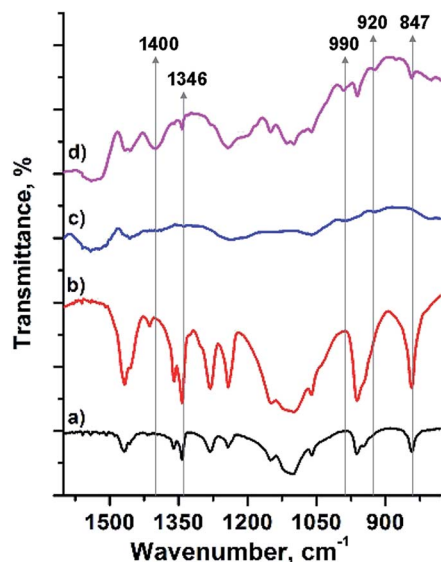
Fig. 4 FTIR spectra of: (a) neat PEO, (b) the PEO/f-G composite film, (c) keratin and (d) the keratin–PEO/f-G composite film.
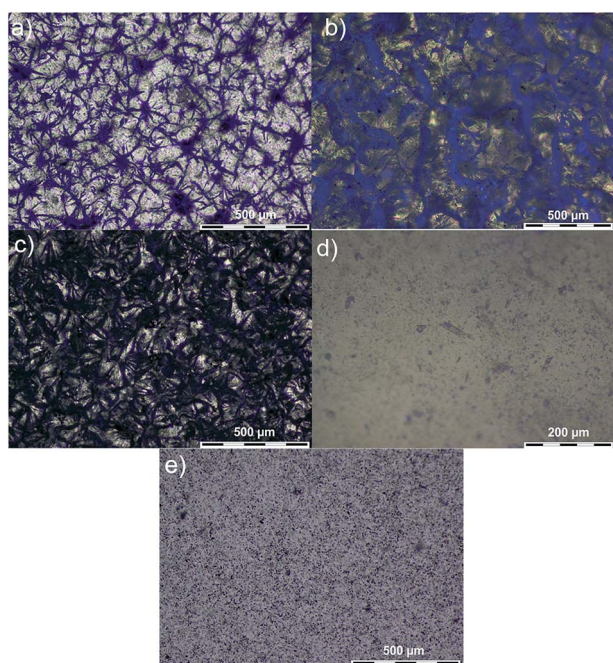

Fig. 5 Optical images of (a) neat PEO, (b) PEO/p-G, (c) PEO/f-G, (d) keratin–PEO and (e) keratin–PEO/f-G.

slight changes of the spherulites, but the SEM images revealed that a smooth surface of PEO/f-G was maintained compared to neat PEO. The morphology of the blend with addition of PEO to keratin remains unchanged because keratin inhibits the crystallization process of PEO; by changing the morphology of spherulites, a total absence of crystallinity with an increase of the keratin content in the keratin–PEO blend is obtained (see Fig. S4 ESI†).[51] Optical images of keratin–PEO and keratin–PEO/f-G show composite films with a uniform structure and SEM

images of these films show a good adhesion of PEO on the keratin fiber surfaces. Addition of f-G supported the morphological structure of the polymer and polymer blend matrix. In the FTIR spectra, we observed intermolecular hydrogen bonding between constituents of both composite films, keratin–PEO and keratin–PEO/f-G, which predicted the thermal stability and increase of mechanical properties of these materials.

4.4. Thermal and mechanical characterization

Thermal analysis of keratin indicates weight loss in water and moisture vaporization below 150 °C, followed by decomposition and destruction of keratin structure up to 400–420 °C.[19] Comparison of the residual mass at 600 °C for addition of f-G to PEO and the polymer blend system indicated an improvement in the thermal stability (Table 1). DSC analysis showed that addition of graphene structures to the polymer led to a decrease in the crystallinity of nanocomposite films, which is in accordance with the work of Shen *et al.* (Fig. 6).[44]

Mechanical properties of composite films were studied using nanoindentation and DMA methods. Measured results of the reduced elastic modulus and hardness are shown in Fig. 7 (see Table S2 ESI†). The addition of a small content (0.3 wt%) of p-G increased the modulus and hardness of the PEO nanocomposite by about 5 and 33%, respectively. Functionalization of graphene significantly increased the composite modulus and hardness by about 92% and 190%, respectively, proving the success of the proposed ultrasonic graphene functionalization. Incorporation of the same content (0.3 wt%) of f-G in the blend of PEO and keratin polymers yielded a significant increase in mechanical properties, *i.e.* the modulus and hardness were increased by 155% and 99%, respectively. Namely, 10 wt% of PEO enables changes in keratin, allowing it to retain high mechanical properties and provide enough elasticity to blended films with a high keratin content.[51,52]

The practical application of keratin based products was limited due to their poor strength and flexibility. Neat keratin films are shown to be too fragile for practical use, but the addition of plasticizers resulted in relatively strong, flexible, and biodegradable films and their potential use as biomaterials in
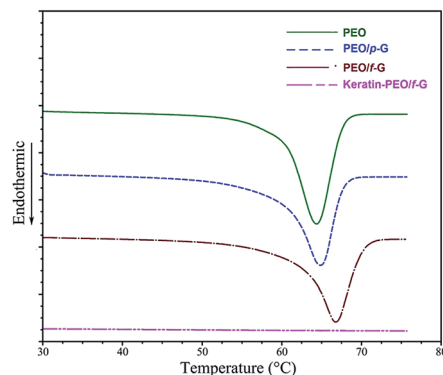

Fig. 6 DSC analysis of (a) PEO, (b) PEO/p-G, (c) PEO/f-G, and (d) keratin–PEO/f-G.
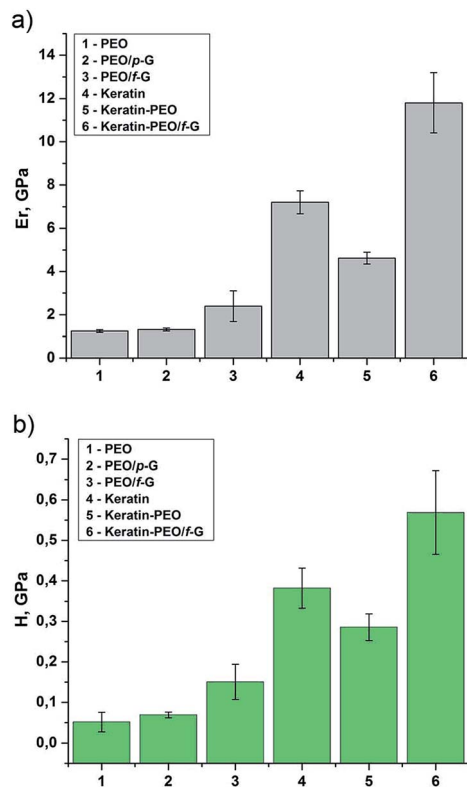
Fig. 7   Nanoindentation measurements of (a) reduced elastic modulus and (b) indentation hardness.
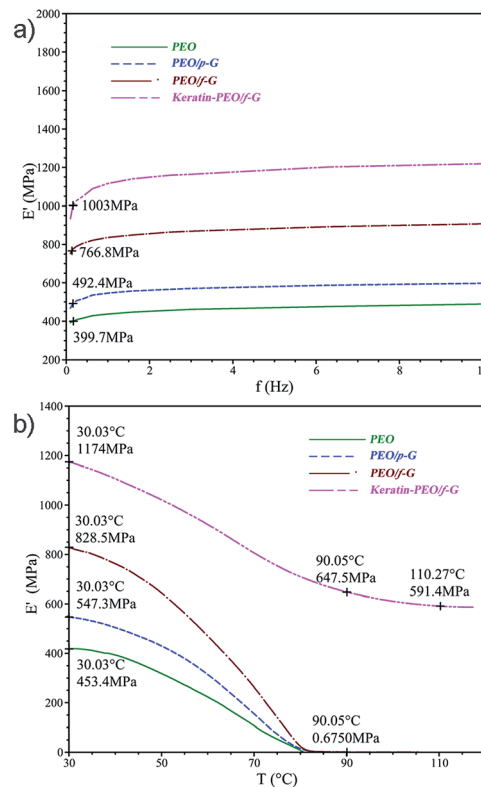

Fig. 8   DMA in the (a) multi frequency and (b) temperature modes for neat PEO and composite films.

medical applications. We also investigated alternative preparation techniques for creating keratin films with more suitable mechanical properties in addition to creating blended keratin systems with PEO polymers. Because of all the above, material properties of neat keratin and blends with a high content of keratin are measured only by nanoindentation since the fragile nature of keratin does not enable proper boundary conditions for DMA measurement. The addition of reinforcements, in the form of p-G and f-G, enables DMA testing in a proper manner.[51,54] Incorporation of a small content of PEO (10 wt%) and f-G (0.3 wt%) increased the keratin modulus and hardness by about 64 and 49%, respectively. It is worth noting that the use of 90 wt% keratin, as a waste abundant material, leads to a remarkable enhancement of mechanical properties. The benefits of such an approach are two fold, namely, the use of a bio-waste component contributes to a more advanced material and on the other hand, this could lead to the use of a significant amount of waste material for the fabrication of materials with added value. The improvement of basic polymer mechanical properties is achieved by introducing materials of increased stiffness (keratin and especially graphene), a change in the crystallinity of polymer systems, a more effective distribution and exfoliation of graphene flakes in polymer matrices and bonding of the particle and matrix phases.[37,42,53]

The storage modulus of neat PEO and blend composite films was determined as a function in the multi frequency and temperature modes (Fig. 8). Due to the polymer crystallinity,

PEO and keratin show an affinity for polymorphic modifications, which represent the ability of the material to change its crystal orientation and crystallinity phases with an applied tension force.[55] A slight increase of the storage modulus in the multi frequency mode is a result of the orienting crystalline phases of PEO and nanocomposite films. Several studies about overcoming the fragile nature of keratin indicated the potential for producing films and fibers with a high content of keratin with PEO.[12,51] Nanoindentation measurements demonstrated changes in mechanical properties of the keratin–PEO blend (see Fig. S5 ESI†) and in accordance with nanoindentation results and the inability of measuring films with a high keratin content, DMA is used to emphasize the influence of f-G. Addition of p-G increases the storage modulus by 23%. Also addition of only 0.3 wt% f-G provided an increase of 92% in the storage modulus compared to neat PEO, while keratin–PEO/f-G shows an increase of about 151% due to crystallinity changes. These findings are similar and follow the same trend observed in nanoindentation results, which yielded increases in the reduced modulus of the same composition by about 5, 92 and 155%.

After this measurement the samples were subjected to DMA analysis in the temperature mode, where the storage modulus is presented as a function of temperature (Fig. 8b). After procedure one, E' of the PEO film at 30 °C was 453.4 MPa, which significantly decreased at about 85 °C in the second procedure. The same behavior was shown in the composite films with

a graphene structure (p-G and f-G), with a rapid decrease at about 90 °C. E' of the keratin–PEO/f-G film showed a decreasing trend, but it reached a storage modulus value of about 591.7 MPa towards the end of the investigated temperature range, due to the presence of keratin and its polymorphic modification ability. For the sake of real term applications, the scope of testing was focused on temperatures above 30 °C, in the rubbery region of these materials. At higher temperatures ($T > 70$ °C), the storage modulus of the neat polymer and nanocomposites decreased very sharply due to the melting of the crystalline region in the PEO. Observation of the rubbery plateau above the melting temperature suggests physical crosslinking of the nanocomposite structure with addition of both p-G and f-G (see Fig. S6a ESI†).[54] The tan δ curve of the neat PEO and nano-composites as a function of the temperature is presented in the ESI (see Fig. S6b†). The tan δ peak magnitude of nano-composites compared to the magnitude of the neat polymer decreases after loading of graphene and keratin, in the range of 0.49 to 0.13 (at 90 °C). There are very small changes of the storage modulus and tan δ in the rubbery region of the keratin–PEO/f-G sample. This probably happens because keratin inhibits the PEO crystallization process and PEO interferes with the keratin self-assembly at the appropriate level by inducing a protein structure with high thermal stability.[51]

The results of this study demonstrated the possibility of fabrication of composite blend films with a high content of keratin from chicken feather waste. To overcome the fragile nature of neat keratin, blending keratin with a small content of PEO and incorporating ultrasonically treated graphene produces films with remarkable mechanical properties, revealing the possibility of using widely available bio-waste materials, such as keratin, for fabrication of functional materials with added value.

5. Conclusion

This study confirmed ultrasonic irradiation as an effective method for grafting PEO onto a graphene surface. Keratin–PEO/f-G bio-nanocomposite films have been successfully fabricated by the solvent casting method. Compared to neat PEO, addition of f-G showed an increase of 92% in the storage and reduced moduli, observed in DMA and nanoindentation results. Nano-indentation testing showed that the incorporation of 0.3 wt% f-G increased the reduced modulus and hardness of the keratin–PEO blend by about 155 and 99%, respectively. The reinforce-ment is generated due to crystallinity changes and the effective load transfer between the reinforcing and matrix phases. These findings open possibilities for the utilization of abundant waste keratin for fabrication of new materials with significantly improved mechanical properties.

Acknowledgements

References

1 M. A. Khosa and A. Ullah, *Journal of Food Processing & Beverages*, 2013, **1**, 1–8.

2 H. K. Ahn, M. S. Huda, M. C. Smith, W. Mulbry, W. F. Schmidt and J. B. Reeves III, *Bioresour. Technol.*, 2011, **102**, 4930–4933.

3 A. J. Poole, J. S. Churc and M. G. Huson, *Biomacromolecules*, 2009, **10**, 1–8.

4 X. C. Yin, F. Y. Li and R. M. Wang, *Biomater. Sci.*, 2013, **1**, 528–536.

5 A. Aluigi, C. Tonetti, C. Vineis, C. Tonin and G. Mazzuchetti, *Eur. Polym. J.*, 2011, **47**, 1756–1764.

6 P. Kar and M. Misra, *J. Chem. Technol. Biotechnol.*, 2004, **79**, 1313–1319.

7 S. Balaji, R. Kumar, R. Sripriya, P. Kakkar, D. Vijaya Ramesh, P. Neela Kanta Reddy and P. K. Sehgal, *Mater. Sci. Eng., C*, 2012, **32**, 975–982.

8 I. Spiridon, O. M. Paduraru, M. F. Zaltariov and R. N. Darie, *Ind. Eng. Chem. Res.*, 2013, **52**, 9822–9833.

9 S. Cheng, K. Lau, T. Liu, Y. Zhao, P. M. Lam and Y. Yin, *Composites, Part B*, 2009, **40**, 650–654.

10 J. G. Rouse and M. E. van Dyke, *Materials*, 2010, **3**, 999–1014.

11 K. Arai and K. Hagiwara, *Int. J. Biol. Macromol.*, 1980, **2**, 355–360.

12 A. L. Martinez-Hernandez and C. Velasco-Santos, *Keratin: structure, properties and applications*, Nova Science Publishers, Inc., Hauppauge, HY, USA, 2012, ch. 7, pp. 149–211.

13 A. Aluigi, A. Varesano, A. Montarsolo, C. Vineis, F. Ferrero, G. Mazzuchetti and C. Tonin, *J. Appl. Polym. Sci.*, 2007, **104**, 863–870.

14 A. Aluigi, C. Vineis, A. Varesano, G. Mazzuchetti, F. Ferrero and C. Tonin, *Eur. Polym. J.*, 2008, **44**, 2465–2475.

15 A. Aluigi, C. Tonetti, F. Rombaldoni, D. Puglia, E. Fortunati, I. Armentano, C. Santulli, L. Torre and J. M. Kenny, *J. Mater. Sci.*, 2014, **49**, 6257–6269.

16 S. Akhlaghi, A. Sharif, M. Kalaee, A. Nouri and M. Manafie, *Polym. Int.*, 2012, **61**, 646–656.

17 E. Fortunati, A. Aluigi, I. Armentano, F. Morena, C. Emiliani, S. Martino, C. Santulli, L. Torre, J. M. Kenny and D. Puglia, *Mater. Sci. Eng., C*, 2015, **47**, 394–406.

18 C. D. Tran and T. M. Mututuvari, *Langmuir*, 2015, **31**, 1516–1526.

19 M. Zoccola, A. Aluigi, C. Vineis, C. Tonin, F. Ferrero and M. G. Piacentino, *Biomacromolecules*, 2008, **9**, 2819–2825.

20 Y. Estevez-Martinez, C. Velasco-Santos, A. L. Martinez-Hernandez, G. Delgado, E. Cuevas-Yanez, D. Alaniz-Lumbreras, S. Duron-Toress and V. M. Castano, *J. Nanomater.*, 2013, **2013**, 1–9.

21 C. Rodriguez-Gonzalez, A. L. Martinez-Hernandez, V. M. Castano, O. V. Kharissova, R. S. Ruoff and C. Velasco-Santos, *Ind. Eng. Chem. Res.*, 2012, **51**, 3619–3629.

22 C. Rodriguez-Gonzales, O. V. Kharrisova, A. L. Martinez-Hernandez, V. M. Castano and C. Velasco-Santos, *Dig. J. Nanometer. Bios.*, 2013, **8**, 127–138.

23 G. Ma, Y. Liu, C. Peng, D. Fang, B. He and J. Nie, *Carbohydr. Polym.*, 2011, **86**, 505–512.

24 F. Qu, M. P. Pintauro, J. E. Haughan, E. A. Henning, J. L. Esterhai, T. P. Schaer, R. L. Mauck and M. B. Fisher, *Biomaterials*, 2015, **39**, 85–94.

25 M. S. Akhtar, S. Kwon, F. J. Stadler and O. B. Yang, *Nanoscale*, 2013, **5**, 5403.

26 M. M. Crowley, F. Zhang, J. J. Koleng and J. W. McGinit, *Biomaterials*, 2002, **23**, 4241–4248.

27 S. Ibrahim and M. R. Johan, *Int. J. Electrochem. Sci.*, 2012, **7**, 2596–2615.

28 F. Fraisse, S. Morlat-Therias, J. L. Gardette, J. M. Nedelec and M. Baba, *J. Phys. Chem. B*, 2006, **110**, 14678–14684.

29 M. Park, B. S. Kim, H. K. Shin, S. J. Park and H. Y. Kim, *Mater. Sci. Eng., C*, 2013, **33**, 5051–5057.

30 J. Zainuddin, P. Albinska, P. Ulanski and J. M. Rosiak, *J. Radioanal. Nucl. Chem.*, 2002, **253**, 339–344.

31 P. Blake, P. D. Brimicombe, R. R. Nair, T. J. Booth, D. Jiang, F. Schedin, L. A. Ponomarenko, S. V. Morozov, H. F. Gleeson, E. W. Hill, A. K. Geim and K. S. Novoselov, *Nano Lett.*, 2008, **8**, 1704–1708.

32 W. E. Mahmoud, *Eur. Polym. J.*, 2011, **47**, 1534–1540.

33 M. Pumera, *Mater. Today*, 2011, 14.

34 G. Wang, X. Shen, J. Yao and J. Park, *Carbon*, 2009, **47**, 2049–2053.

35 G. Wang, X. Shen, B. Wang, J. Yao and J. Park, *Carbon*, 2009, **47**, 1359–1364.

36 X. Zhao, Q. Zhang and D. Chen, *Macromolecules*, 2010, **43**, 2357–2363.

37 A. M. Pandele, M. Ionita, L. Crica, S. Dinescu, M. Costache and H. Iovu, *Carbohydr. Polym.*, 2014, **102**, 813–820.

38 G. Carotenuto, S. de Nicola, M. Palomba, D. Pullini, A. Horsewell, T. W. Hansen and L. Nicolais, *Nanotechnology*, 2012, **23**, 485705.

39 M. A. Rafiee, J. Rafiee, Z. Wang, H. Song, Z. Z. Yu and N. Koratkar, *ACS Nano*, 2009, **3**, 3884–3890.

40 S. Stankovich, D. A. Dikin, G. H. B. Dommett, K. M. Kohlhaas, E. J. Zimney, E. A. Stach, R. D. Piner, S. T. Nguyen and R. S. Ruoff, *Nature*, 2006, **442**, 282–286.

41 H. K. F. Cheng, N. G. Sahoo, Y. P. Tan, Y. Pan, H. Bao, L. Li, S. H. Chan and J. Zhao, *ACS Appl. Mater. Interfaces*, 2012, **4**, 2387–2394.

42 M. Ionita, A. M. Pandele and H. Iovu, *Carbohydr. Polym.*, 2013, **94**, 339–344.

43 R. Justin and B. Chen, *Carbohydr. Polym.*, 2014, **103**, 70–80.

44 B. Shen, W. Zhai, D. Lu, J. Wang and W. Zheng, *RSC Adv.*, 2012, **2**, 4713–4719.

45 K. S. Suslick and G. Price, *Annu. Rev. Mater. Sci.*, 1999, **29**, 295–326.

46 H. Xu, B. W. Zeiger and K. S. Suslick, *Chem. Soc. Rev.*, 2013, **42**, 2555–2567.

47 H. Xu and K. S. Suslick, *J. Am. Chem. Soc.*, 2011, **133**, 9148–9151.

48 S. B. Jagtap, R. K. Kushwaha and D. Ratna, *RSC Adv.*, 2015, **5**, 30555–30563.

49 A. Vasconcelos and A. Cavaco-Paulo, *Curr. Drug Targets*, 2013, **14**, 612–619.

50 E. F. Hartree, *Anal. Biochem.*, 1972, **48**, 422–427.

51 C. Tonin, A. Aluigi, A. Varesano and C. Vineis, *Nanofibers, Keratin-based Nanofibres*, InTech, Croatia, 2010.

52 Y. Liu, X. Yu, J. Li, J. Fan, M. Wang, T. D. Lei, J. Liu and D. Huang, *J. Nanomater.*, 2015, **2015**, 1–7.

53 A. M. Diez-Pascual, M. A. Gomez-Fatou, F. Ania and A. Flores, *Prog. Mater. Sci.*, 2015, **67**, 1–94.

54 Y. W. Chang, K. S. Lee, Y. W. Lee and J. H. Bang, *Polym. Bull.*, 2015, **72**, 1937–1948.

55 S. Fakirov and F. J. Balta Calleja, *Handbook of Thermoplastic Polymers: Homopolymers, Copolymers, Blends, and Composites*, Weinheim, 2002.